2019 IEEE Conference on Control Technology and Applications (CCTA)
Hong Kong, China, August 19-21, 2019

Dynamic Inversion Based Navigation Algorithm for Furrow-Traversing Autonomous Crop Rover*

Jeff Hammer and Chong Xu[1]

Abstract— **In this paper, we present a dynamic-inversion based navigation algorithm to autonomously drive the horticulture rover used for precision agriculture purposes along a narrow furrow without damaging the crops. The horticulture rover traverses the furrow by aligning itself with the centerline with the assistance of a real-time kinematic (RTK)-capable GPS as the location sensor. The results of the simulation whose critical parameters are obtained experimentally from the real system have proved that, the rover is able to correct itself back to the centerline of the course within 1 m distance along the furrow and maintain at the centerline with a fluctuation of less than 3 cm even with system uncertainty and noise, after a disturbance causing a lateral offset of 16 cm and a leaving-centerline heading of 2 degrees.**

I. INTRODUCTION

Declining resources and the ever-growing population on the earth have posed increasingly bigger challenges to the farmers, who are impelled to achieve higher crop yields with less resource inputs while preserving the environment [1], [2]. That's why precision agriculture has become a heated research topic in the recent decades [3], [4]. To achieve the above mentioned goal, more and more precise farm machineries are needed to provide reliable agricultural tasks with consistent performance. Autonomous robots are excellent choices for long duration of repetitive tasks. Using electricity as prime power increases power efficiency and reduces the complexity of equipment as well as overall mass.

The Rx Robotics horticultural rover, as shown in Fig. 1, is an electrical powered autonomous vehicular platform that is designed to carry out agricultural tasks such as watering and collecting samples of farmland and crops with little or no human intervention. The samples collected will be processed with trained machine learning algorithms to help the farmers to make decisions regarding agricultural actions (e.g. watering, fertilizing, harvesting, further inspection, etc).

To operate in the field, the bottom-line requirement for any autonomous vehicle is to self navigate along the centerline of the furrow without damaging the crops. A dynamic-inversion based navigation algorithm is proposed in this paper to fulfill the objective. Dynamic inversion algorithm dates back as early as 1987, when Morton [5] and Elgersma [6] first proposed an alternative methodology to the divide-and-conquer approach for flight control problems. A similar strategy called feedback linearization was brought to the public's attention by Brockett [7], Hunt [8] and Isidori [9] at around the same time.

Fig. 1: Rx Robotics autonomous horticultural rover, the 'bikebot'. The rover is currently an electrical powered wheeled vehicle, which will be remodeled with tracks.

Honeywell aerospace engineer Dale Enns [10] has improved the robustness properties of the dynamic inversion algorithm based on the work done by Spong [11], Kravaris [12] and Akhrif [13]. He was dedicated to further evolving the dynamic inversion approach so that it eventually becomes one of the fundamental principles in flight control.

The dynamic inversion algorithm employs a nonlinear approach to globally invert the dynamic equations so that the selected control variables have a linear representation. This strategy bypasses the step of subsystem separation and gain scheduling, which take up huge amount of resources keenly desired in any real-time system. In recent years, more and more researchers have devoted to further developing and applying the dynamic inversion based algorithms for aircraft tracking [14], integration with neural network [15], path-planning [16] and path-following [17], etc.

In this paper, we will adopt the dynamic inversion principle to design a navigation algorithm that can accurately control the course of an autonomous electrical crop rover, as shown in Figure 1, to always maintain at the centerline of the furrow. The rover will always return to the centerline of the furrow, with a pre-set trajectory of a mass-damping-spring second order system after a disturbance despite the presence of the noise.

As opposed to the common waypoint-based navigation algorithm which only corrects the heading error, the path-following based dynamic inversion algorithm will correct

* Research is partially sponsored by Rx Robotics LLC, Red Wing, MN, US.

[1] Both Authors are with the School of Engineering, University of St. Thomas, Twin Cities, MN 55105, USA chong.xu@stthomas.edu

both the heading and lateral error. It has its advantage over traditional waypoint-based navigation algorithm in terms of its narrower and predefined correcting course and robustness to model uncertainty and noise. Hence, the error-correction course enforced by the dynamic inversion based control algorithm will be faster convergent with less oscillation around the centerline of the furrow when the parameters of the control algorithm are carefully selected. Moreover, the dynamic inversion based algorithm architecture can be developed into advanced control elements and will enable further control research into adaptive controls and the control of flexible structures.

The problem background and rove kinematic equations will be given in Section II. The dynamic model designed to be the self-correction course of the rover is given in Section III, and the control variable is selected and formulated according to the rule of dynamic inversion. The final form of all the control variables in the system and the state-space representation of the close-loop speed control subsystems are given in Section IV. Finally simulation results with experimentally obtained parameter values are given in Section V. The selection of key parameter values of the algorithm will also be discussed in Section V. Last but not the least, the paper will be concluded in Section VI.

II. NOMENCLATURE AND ROVER KINEMATIC

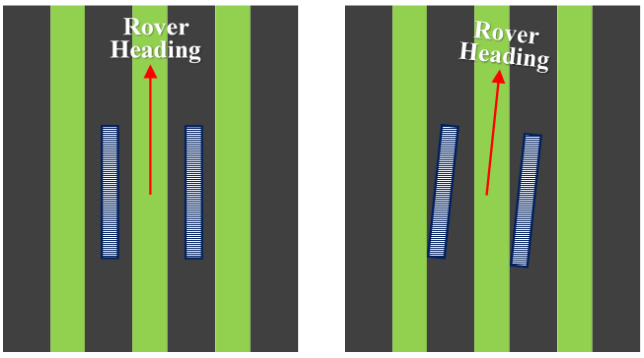

(a) Aligned (b) Misaligned

Fig. 2: Top view illustration of crop furrows and rover: (a) Rover is aligned with the centerline of the furrow, with zero cross-track and heading errors; (b) Rover is misaligned with the centerline of the furrow, with negative cross-track error and positive heading error.

Figure 2 shows a top view of the crops, furrow and the two tracks of the autonomous rover. The vertical green bars represent the rows of crops. The vertical black bars represent the space between the rows of growing crops i.e. the dirt furrow. The short white bars with horizontal-line pattern fillings are the left and right tracks of the rover. The red arrow is the velocity vector of the rover, starting from the center of the rover. In Figure 2a, the rover is correctly positioned with its lateral center aligned with the horizontal middle of a furrow where its payload can operate properly. The heading is parallel to the furrows as it should be when there is no heading error. The navigation and control design must restore the rover to this alignment in the field after a cross-track and/or heading error are generated by some disturbance. Figure 2b shows the rover with a negative cross-track error

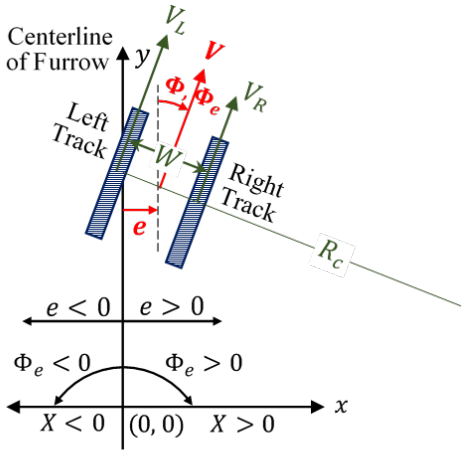

Fig. 3: Illustration of cross-track error e and heading error Φ_e, as well as the geometric relationship of the motion of the rover, when the furrow is assumed to be straight around the rover.

and a positive heading error.

As shown in Figure 3, the cross-track error e is defined as the normal distance from the centerline of the furrow to the rover center, with right offset being positive. The heading error Φ_e is the angular difference between the heading of the rover and heading of the furrow. The heading error is positive, if the rover is skewed clockwise from the heading of the centerline of the furrow.

The cross-track error shown in Figure 2b is negative and the heading error is positive and in the correct direction to cause the rover to go back towards the center of the furrow. If the rover turned more than this to correct the error, the tracks would damage the adjacent crops. So the trajectory of the rover after a disturbance must remain nearly parallel to the rows to minimize crop damage. The requirement is the navigation and control system shall cause the rover to move from this attitude back to the centerline without damaging the crops.

From the geometry displayed in Figure 2, the motion of the two-track autonomous rover can be modeled as the following simplified nonholonomic system:

$$\begin{cases} \dot{X} &= V\sin\Phi \\ \dot{Y} &= V\cos\Phi \\ V &= \dot{\Phi}R_c \\ V_L &= \dot{\Phi}\left(R_c+\dfrac{W}{2}\right) = V+\dot{\Phi}\dfrac{W}{2} \\ V_R &= \dot{\Phi}\left(R_c-\dfrac{W}{2}\right) = V-\dot{\Phi}\dfrac{W}{2} \end{cases}, \tag{1}$$

where W is the width between the two tacks, and V_L, V_R are the left and right track speeds respectively. Φ is the heading of the rover with respect to the furrow. It is the same as Φ_e

when the furrow is assumed to be straight around the rover, .

Therefore, adding V_L and V_R will achieve

$$V_L + V_R = \dot{\Phi}\left(R_c + \frac{W}{2}\right) + \dot{\Phi}\left(R_c - \frac{W}{2}\right) = 2\dot{\Phi}R_c = 2V. \tag{2}$$

Hence, the actual speed of the rover V can be calculated from the measurements of the left and right track speeds as

$$V = \frac{V_L + V_R}{2}. \tag{3}$$

Similarly, subtracting V_R from V_L will achieve

$$V_L - V_R = \dot{\Phi}\left(R_c + \frac{W}{2}\right) - \dot{\Phi}\left(R_c - \frac{W}{2}\right) = \dot{\Phi}W. \tag{4}$$

Therefore, the actual turning rate of the rover $\dot{\Phi}$ can be evaluated from the measurements of the left and right track speeds as:

$$\dot{\Phi} = \frac{V_L - V_R}{W}. \tag{5}$$

III. DYNAMIC INVERSION BASED NAVIGATION

In order to make the crop rover self-maneuver through the narrow furrow without damaging the crops, we proposed a system architecture including a navigation subsystem and two independent speed control subsystems for the two tracks, as shown in Figure 4.

The goal of designing the navigation system is to reduce the cross-track error e, its first and second order derivative $\dot{e}$ and $\ddot{e}$ to zero after a disturbance. Meanwhile, the course of the rover during the e-reduction process needs to be carefully designed to be narrow enough, so that the rover won't run over the crops. To achieve this goal, the cross-track error e is designed to act like the displacement of a spring-mass-damper system, whose behavior can be modeled by the following second order differential equation [18]:

$$\ddot{e} + 2\zeta\omega_n\dot{e} + \omega_n^2 e = 0, \tag{6}$$

where ζ is the damping ratio, and ω_n is the natural frequency. No matter what is the initial value of the cross-track error e after disturbance, if the physical behavior of e can follow the differential equation in Equation (6), the value of cross-track error e and its first/second order derivative will die out to zero after approximately

$$T_s = \frac{4}{\zeta\omega_n} \tag{7}$$

seconds. On the other hand, according to Figure 3, we have

$$\dot{e} = V\sin\Phi_e = V\Phi_e \quad \text{for small } \Phi_e \tag{8}$$

and hence when $\dot{e}$ controlled by Equation (6) settles down to zero, the heading error Φ_e will also die out to zero. According to Equation (8), the second order derivative of cross-track error e is

$$\ddot{e} = \frac{d(V\Phi_e)}{dt} = \dot{V}\Phi_e + V\dot{\Phi}_e = \dot{V}\Phi_e + V\left(\dot{\Phi} - \dot{\Phi}_{\text{row}}\right) \tag{9}$$

Substituting the left hand side of Equation (6) with Equations (8) and (9), we have

$$\dot{V}\Phi_e + V\left(\dot{\Phi} - \dot{\Phi}_{\text{row}}\right) + 2\zeta\omega_n V\Phi_e + \omega_n^2 e = 0 \tag{10}$$

Selecting the commanded turning rate $\dot{\Phi}$ as the control variable and applying the dynamic inversion rule [10], we have:

$$\dot{\Phi}_{\text{set}} = \frac{V\dot{\Phi}_{\text{row}} - \dot{V}\Phi_e - 2\zeta\omega_n V\Phi_e - \omega_n^2 e}{V}, \tag{11}$$

where all the variables at the right hand side of Equation (11) can be obtained through sensor measurements and the left hand side is the command variable, which will be used to calculate the left and right track speed setpoints. Notice since the speed V is in the denominator, Equation (11) applies only for finite speed. At zero speed, it is singular.

IV. SIMPLIFIED CONTROL VARIABLES AND COMPLETE MODEL

For most furrows, we will assume that the furrow is roughly straight or the changing rate of the furrow is slow enough as compared to the speed of the rover, so that it can be regarded as a straight line at any point. Thus we will have $\dot{\Phi}_{\text{row}} = 0$. By further substituting ω_n with Equation (**??**) in the Equation (11), we will have the setpoint of the control variable turning rate as,

$$\dot{\Phi}_{\text{set}} = -\frac{\dot{V}}{V}\Phi_e - V\left(2\frac{\Phi_e}{Y_0} + \frac{e}{\zeta^2 Y_0^2}\right). \tag{12}$$

This will be used to set the left and right track desired speed $V_{L,\text{set}}$ and $V_{R,\text{set}}$. According to the basic kinematic model shown in Equation (1), we have

$$\begin{cases} V_{L,\text{set}} &= V_{\text{set}} + \dot{\Phi}_{\text{set}}\dfrac{W}{2} \\ V_{R,\text{set}} &= V_{\text{set}} - \dot{\Phi}_{\text{set}}\dfrac{W}{2} \end{cases}, \tag{13}$$

where V_{set} is the commanded speed of the rover. We want the rover to speed up at the beginning of the furrow, reach and stay at the maximum speed and then slow down to stop at the end of the furrow. Following this strategy, the total length of the furrow L subtracting the distance Y traveled by the rover along the furrow is designed to reduce to zero like the displacement of a mass with spring and damper:

$$\frac{d^2(L-Y)}{dt^2} + 2\zeta_{\text{stop}}\omega_{n,\text{stop}}\frac{d(L-Y)}{dt} + \omega_{n,\text{stop}}^2(L-Y) = 0, \tag{14}$$

with ζ_{stop} and $\omega_{n,\text{stop}}$ being the damping ratio and natural frequency of the second order system. As $d^2L/dt^2 = dL/dt = 0$ and with the heading error Φ_e being small, we may assume that the rover speed along the furrow V_y equals to the rover speed V. Thus according to the rule of dynamic inversion [10], we will have the control variable, the commanded acceleration set as

$$a_{\text{set}} = -2\zeta_{\text{stop}}\omega_{n,\text{stop}}V + \omega_{n,\text{stop}}^2(L-Y). \tag{15}$$

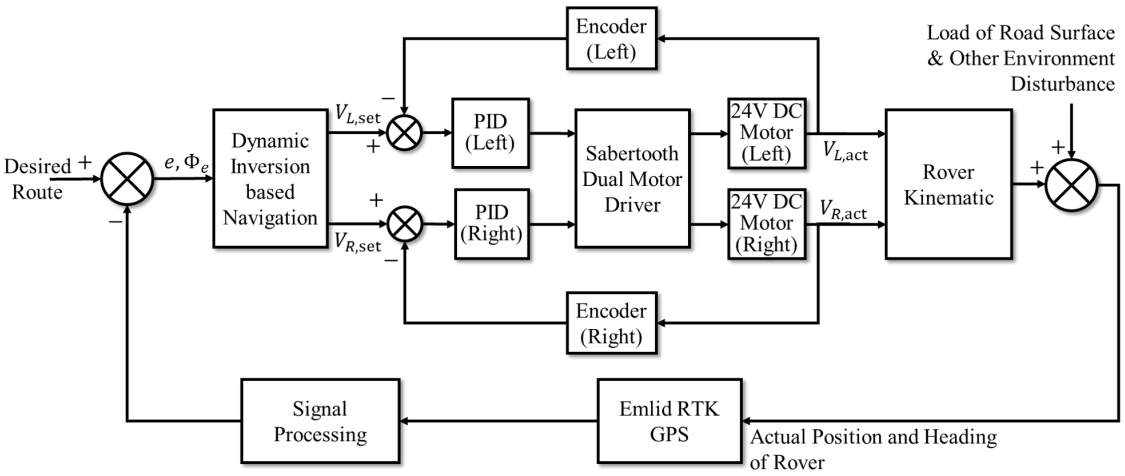

Fig. 4: System block diagram of the two-track electrical-motor driving autonomous crop rover.

The commanded desired speed of the rover will then be the integration of the desired acceleration. That is

$$V_{\text{set}} = \int a_{\text{set}} dt = \int \left[-2\zeta_{\text{stop}}\omega_{n,\text{stop}} V + \omega_{n,\text{stop}}^2 (L - Y)\right] dt. \tag{16}$$

Finally, substituting V_{set} and $\dot{\Phi}_{\text{set}}$ in Equation 13 with Equations (16) and (12), we will achieve the values of the desired left and right track speeds.

As can be seen from the system architecture in Figure 4, PID controllers are adopted to constantly adjust the actual speeds of the left and right tracks to the commanded setpoint. For both the left and right tracks, the model from $V_{L/R,\text{set}}$ to $V_{L/R,\text{act}}$ can be expressed as

$$\dot{\mathbf{V}}_{\mathbf{L/R},\text{act}} = \mathbf{S}\mathbf{V}_{\mathbf{L/R}}, \tag{17}$$

where

$$\begin{aligned} \dot{\mathbf{V}}_{\mathbf{L/R},\text{act}} &= [\dot{V}_{L/R,\text{act}} \quad \ddot{V}_{L/R,\text{act}}]^T \\ \mathbf{V}_{\mathbf{L/R}} &= [V_{L/R,\text{act}} \quad \dot{V}_{L/R,\text{act}} \quad V_{L/R,\text{set}} \quad \dot{V}_{L/R,\text{set}}]^T, \end{aligned} \tag{18}$$

and $\mathbf{S}$ is the transition matrix. For the simulation we proceed, we assume that the left and right track have the same transition matrix. From the experimental tests taken with the rover shown in Figure 1, we have the following values of the transition matrix both for left and right tracks.

$$\mathbf{S} = \begin{bmatrix} 0 & 1 & 0 & 0 \\ -11.85 & -6.523 & 11.85 & 1.317 \end{bmatrix} \tag{19}$$

V. SIMULATION RESULTS

A. Noise-Free Simulation

In Subsection V-A, we are going to present the simulation results of the system seen in Figures 1 and 4, when the noise is assumed to be zero at any place. The parameters of all the equations introduced in Sections II∼IV are listed in Table I, which are used in the simulation to generate all the figures in Section V.

During the simulation process, the up-bounds of the control variables in Equations (13), (15) and (16) are set to be $|\dot{\Phi}_{\text{set}}| < \dot{\Phi}_{\max}$, $|a_{\text{set}}| < a_{\max}$ and $|V_{\text{set}}| < V_{\max}$, whose values are given in Table I. The initial cross-track error and heading error are assumed to be $e = -16$ cm and $\Phi_e = -5^\circ$ for Figure 5 and Figure 6.

TABLE I: Parameters used for simulations that generate all the figures in Section V.

Sampling Period	dt	0.05 second
Rover Width	W	0.9 m
Length of Furrow	L	100 m
Maximum Turning Rate	$\dot{\Phi}_{\max}$	1 rad/sec
Maximum Acceleration	$a_{\max}$	1 m/s^2
Maximum Rover Speed	$V_{\max}$	1.5 m/s
Damping Ratio Along Furrow	ζ_{stop}	0.9
Natural Frequency Along Furrow	$\omega_{n,\text{stop}}$	1 rad/sec

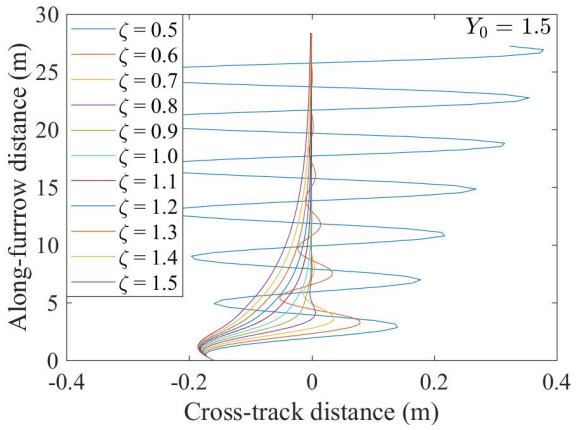

Fig. 5: Simulation results of the trajectory of the rover in Figure 1 following the centerline of a furrow, when the convergence distance Y_0 is set to be 1.5, and the damping ratio ζ varies from 0.5 to 1.5. The noise is assumed to be absent when results are obtained.

As can be seen in Figure 5, when the convergence distance is fixed at a certain value, the bigger the damping ratio

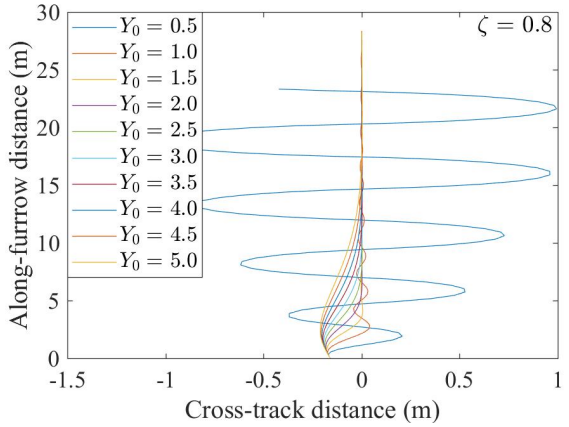

Fig. 6: Simulation results of the trajectory of the rover in Figure 1 following the centerline of a furrow, when the damping ratio ζ is set to be 0.8, and convergence distance Y_0 varies from 0.5 to 5.0. The noise is assumed to be absent when results are obtained.

ζ, the slower the trajectory returns to the centerline of the furrow. However, at the same time, the less the trajectory will oscillate. Though according to the dynamic of the second order system, the system should always be stable despite the value of damping ratio ζ, the simulation result shows that when the convergence distance along furrow is set to be $Y_0 = 1.5$ m, damping ratio $\zeta = 0.5$ is making the close-loop system shown in Figure 4 unstable.

This is because the commanded left and right track speeds cannot be achieved instantly. According to the experimental results, it takes approximately 2 seconds for the rover to settle down at a given desired speed. This delay causes the system to be unstable if the second-order system designed to be inverted to get the control variables are not damped enough. This may be improved by adopting a combinative feed-forward and PID controlling algorithm. Nevertheless, as for the current control algorithm, the damping ratio cannot be too low. The best damping ratio value from the simulation under $Y_0 = 1.5$ m seems to be $\zeta = 0.8$.

Figure 6 presents the simulated trajectories of the rover when damping ratio ζ is fixed to be 0.8, and the convergence distance along the furrow Y_0 varies from 0.5 m to 5.0 m. As can be expected, the shorter the convergence distance, the quicker the rover will return back to the centerline of the furrow, though at a risk of resulting in oscillatory or even unstable trajectory.

The simulation result in Figure 6 shows that when the damping ratio of the dynamic to be inverted is fixed to be $\zeta = 0.8$, a too small convergence distance of $Y_0 = 0.5$ m will make the system unstable. Nevertheless, a too big convergence distance such as $Y_0 = 5$ m will cause the rover to take as long as 15 m to return back to the desired path. This will potentially constitute a bigger issue when the rover is traversing a short leg of less than 15 m and a pivot turn is required at the end of the leg. Examining through all the values of Y_0, it seems that the best value for $\zeta = 0.8$ is $Y_0 = 1.5$ m.

B. Noise Contaminated Simulation

TABLE II: Standard deviation of noises used for simulations that generate all the figures in Subsection V-B.

Cross-Track Error Measurement	$\sigma(e_{\text{mea}})$	0.015 m
Heading Error Measurement	$\sigma(\Phi_{e,\text{mea}})$	1°
Disturbance of the road surface to the left track speed	$\sigma(V_{L,\text{act}})$	0.02 m/s
Disturbance of the road surface to the right track speed	$\sigma(V_{R,\text{act}})$	0.02 m/s
Left Track Speed Measurement	$\sigma(V_{L,\text{act,mea}})$	0.001 m/s
Right Track Speed Measurement	$\sigma(V_{R,\text{act,mea}})$	0.001 m/s

To make the tests more realistic, noise are taken into account in our simulations that generate all the figures in Subsection V-B. All the noises are considered to be white Gaussian distributed, with zero means and standard deviations taking values from Table II. All the noise-levels quantified by the standard deviations in Table II are experimentally obtained. Among them, the measurement of the cross-track and heading errors are obtained with the Emlid real-time-kinematic (RTK) GPS. The noise level of cross-track and heading error measurements in Table II also assumes that the a priori coordinates information of each segment point on the furrow is known. This assumption is of course hard to achieve in reality. Thus, a novel position-detection algorithm is proposed in [19], which doesn't require any a priori information yet achieves comparable detection resolution.

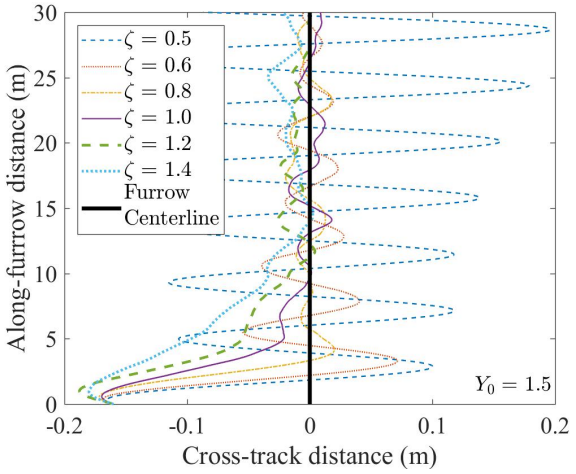

Fig. 7: Simulation results of the trajectory of the rover in Figure 1 following the centerline of a furrow, when the convergence distance Y_0 is set to be 1.5, and the damping ratio ζ varies from 0.5 to 1.4. The noise of the simulation system are assumed to be the values obtained through experimental results as shown in Table .

Figures 7 and 8 is the simulated trajectory of the rover, when the initial cross-track and heading errors are $e = -16$ cm and $\Phi_e = -2^\circ$ and with noise considered. As can be seen from both figures, the same trend is observed as their

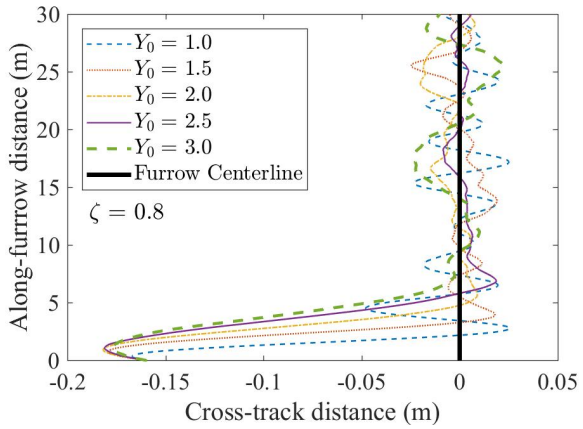

Fig. 8: Simulation results of the trajectory of the rover in Figure 1 following the centerline of a furrow, when the damping ratio ζ is set to be 0.8, and convergence distance Y_0 varies from 1.0 to 3.0. The noise of the simulation system are assumed to be the values obtained through experimental results as shown in Table .

noise-free counterparts. That is, a smaller damping ratio ζ and convergence distance Y_0 will guarantee a sooner return of the rover to the centerline, but not necessarily a sooner convergence, due to non-negligible oscillations and even instability.

It may be worth noting that the scales of the x and y axes are drastically different in all four Figures 5∼8 . This may cause the readers to have a mistaken view of how big the deviation of the rover is from the centerline. As a matter of fact, the fluctuation around the centerline due to noise is less than 3 cm when the furrow width is 76.2 cm (30 inch). Hence, the rover is able to autonomously self-correct its initial errors and go through a visually straight line along the furrow without damaging the crops despite the presence of noise.

VI. CONCLUSIONS

A dynamic-inversion based controlling solution set is developed and applied to navigate the autonomous electrical rover through the centerline of the narrow furrow without damaging the crops. The simulation results based on the parameters of the realistic model, whose values are obtained experimentally, proved that the algorithm is able to successfully correct the course of the autonomous rover with an initial lateral offset of 16 cm and a leaving-centerline heading of 2 degrees back to the centerline within 1 meter. Moreover, the rove is able to maintain around the centerline of the furrow with a standard deviation of less than 3 cm from the centerline, even with the disturbance of the system noise.

ACKNOWLEDGMENT

The authors would like to thank Mr. Scott Morgan and Peter Farley for their financial and technical support to this work.

REFERENCES

[1] J. A. Howard and C. W. Mitchell, Phytogeomorphology, Wiley, 1985.
[2] A. B. McBratney and M. J. Pringle, "Estimating average and proportional variograms of soil properties and their potential use in precision agriculture," Precision Agriculture, Volume 1, Issue 2, pp 125-152, September 1999.
[3] T.C. Kaspar, T. S. Colvin, B. Jaynes, D. L. Karlen, D. E. James and D. W Meek, "Relationship between six years of corn yields and terrain attributes," Precision Agriculture, Volume 4, pp 87-101, 2003.
[4] A. B. McBratney, B. Whelan and T. Ancev, "Future Directions of Precision Agriculture," Precision Agriculture, 6, 7-23, 2005.
[5] B. G. Morton, M. R. Elgersma, C. A. Harvey and G. Hines, "Nonlinear flying quality parameters based on dynamic inversion," AFWAL-TR-87-3079, 1987.
[6] M. R. Elgersma, "Control of nonlinear systems using partial dynamic inversion," Ph.D Dissertation, University of Minnesota, Aprial, 1988.
[7] R. W. Brockett, "Feedback invariants for nonlinear systems," IFAC Congress, Helsinki, 1978.
[8] L. R. Hunt and R. Su, "Control of nonlinear time-varying systems," Proceedings of the IEEE Conference on Decision and Control, December, 1981.
[9] Isidori, A Nonlinear Control Systems: An Introduction, Springer-Verlag, 1985.
[10] D. Enns, D. Bugajski, R. Hendrick, G. Stein, "Dynamic inversion: an evolving methodology for flight control design", International Journal of Control, vol. 59, Issue 1, 1994, pp. 71-91.
[11] M. W. Spong and M. Vidyasagar, "Robust linear compensator design for nonlinear robotic control," IEEE Journal of Robotics and Automation, 3(4), 1987.
[12] C. Kravaris, "On the internal stability and robust design of globally linearizing control systems, " Proceedings of American Control Conference, 1987.
[13] O. Akhrif and G. L. Blankenship, "Robust stabilization of feedback linearizable systems," Proceedings of the IEEE Conference on Decision and Control, 1988.
[14] W. MacKunis, P. M. Patre, M. K. Kaiser and W. E. Dixon, "Asymptotic tracking for aircraft via robust and adaptive dynamic inversion methods", IEEE Transactions on Control Systems Technology, vol. 18, No. 6. November 2010, pp. 1448-1459.
[15] K. Qian and Z. Chen, "Dynamic inversion based on neural network applied to nonlinear flight control system," Proceedings of the 2010 2nd International Conference on Future Computer and Communication, 2010.
[16] C, G. L. Bianco, A. Piazzi and M. Romano, "Smooth motion generation for unicycle mobile robots via dynamic path inversion", IEEE Transactions on Robotics, vol. 20, No. 5, October 2004, pp. 884-891.
[17] L. Cconsolini, A. Piazzi and M. Tosques, "A dynamic inversion based controller for path following of car-like vehicles," IFAC Congress, Barcelona, Spain, 2002.
[18] Norman S. Nise, *Control Systems Engineering (6 edition)*, John Wiley & Sons, Inc.
[19] Langan D., Vraa R., and Xu C, "Machine-vision based location detection solutions for autonomous horticulture rover during early growth season",*Proceedings of IEEE International Conference on Intelligence and Safety for Robotics*, August 24-27, 2018, Shenyang, China.